BIT Numerical Mathematics
2003, Vol. 43, No. 1, pp. 001–018
0006-3835/03/4301-0001 $16.00

Absorbing Boundary Conditions and Optimized Schwarz Waveform Relaxation

L. HALPERN[1]

[1] *LAGA-Institut Galilée -Université Paris 13. Avenue J.B. Clément, 93430 Villetaneuse. France. email: halpern@math.univ-paris13.fr*

Abstract.

We show here how the formalism, introduced by B. Engquist and A. Majda for absorbing boundary conditions, is a powerful tool to produce absorbing boundary layers and Schwarz Waveform Relaxation algorithms, when coupled with best approximation. The demonstration is given on the advection diffusion equation, but the ideas apply also to hyperbolic problems.

AMS subject classification (2000): 65F20.

Key words: Advection-diffusion, absorbing boundaries, Schwarz Waveform Relaxation.

1 Introduction.

One of the main goals in today's computation is the coupling of different models of very large size with various scales both in space and time. Let us mention three of those, related to flow problems. First a combustion process, where the scales of the physico-chemistry reactions can be very different from one to another, see Figure 1.1. The characteristic scales of the flame can only be taken into account by direct simulation (DNS). As full three dimensional fine computations are impossible to run, domain truncation and model coupling with varying space-time scales are essential.

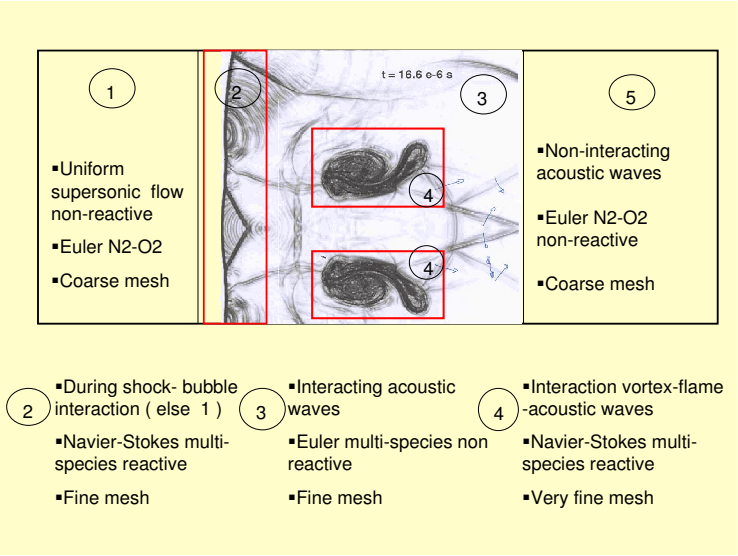

Figure 1.1: A combustion process: hydrogen bubble hitting a supersonic shock. G. Billet, J. Ryan (ONERA, France)

Another example is in environmental science, in the context of nuclear waste disposal simulations, see Figure 1.2. The convection and diffusion constants in the models are very different according to the layer: for example, there is almost no convection in the clay. Furthermore the radioactive elements will be leaking during a very small period, while the computation has to run over a time span of millions of years. The third concern is in oceanography, where various models should be used depending on the zone, as for instance along the Gulf-Stream, close to the Gibraltar channel, *etc.* We would also like to write a coupling algorithm for a local ocean-atmosphere model.

As can be seen from these examples, the various coupling processes are the following:

♢ Truncate the domain with absorbing layers.

♢ For a given problem, split the domain, with domain decomposition algorithm.

♢ For a given problem, use different numerical methods in different zones, like finite elements/finite differences methods, spectral method/finite elements method, adaptive mesh refinement.

♢ Simplify a model in some geographical zone, like boundary layer/Navier-Stokes.

♢ Couple two different models in different zones, like shallow water/primitive equations, ocean/atmosphere.

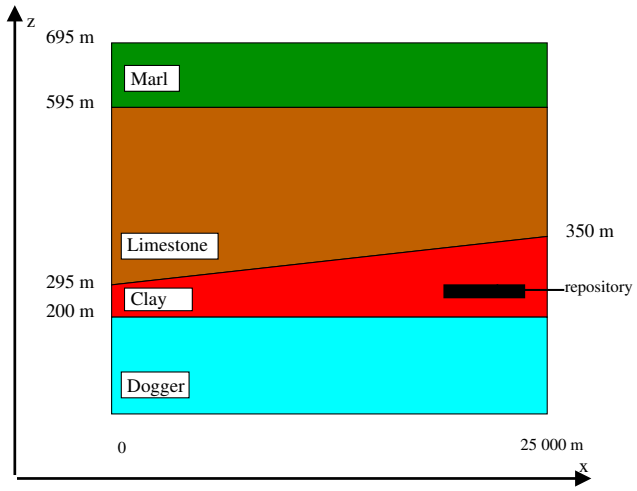

Figure 1.2: Couplex benchmark: a nuclear waste disposal. M. Kern (INRIA, France).

♢ Refine the mesh both in time and space.

For these problems, we define a unified frame, relying on the strategy of absorbing boundary conditions, as developed for hyperbolic problems by B. Engquist and A. Majda [3] , and for parabolic problems in [7]. The material of this presentation concerning domain decomposition algorithms is mainly the fruit of a collaboration with M.J. Gander (University of Geneva, Switzerland).

We work here on parabolic equations, namely the advection diffusion equation, and we describe optimized absorbing layers, and optimized Schwarz Waveform Relaxation algorithms.

2 The problems involved.

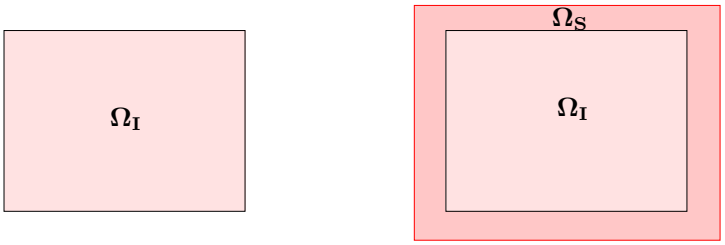

Domain of interest Ω_I Domain of computation $\Omega_C = \Omega_I \cup \Omega_S$

Figure 2.1: Absorbing layer.

Domain of interest Ω_I Split Domain

Figure 2.2: Domain decomposition with overlap

In the first case, we search for a boundary condition on the external boundary of the layer such that the error in the domain of interest is as small as possible: the transparent boundary condition. In the second case, we write an algorithm which solves alternatively in Ω_1 and Ω_2, and we search for transmission conditions on the interfaces, such that the algorithm is as fast as possible: the optimal transmission conditions. We shall see that these problems are closely related. We then replace the optimal methods by approximate ones, using best approximation methods.

3 The absorbing boundary conditions for the advection-diffusion equation.

We consider the advection diffusion equation in $\mathbb{R} \times \mathbb{R}^{n-1} \times (0,T)$

$$\begin{cases} \mathcal{L}(u) := \partial_t u + a\partial_1 u + b \cdot \nabla_y u - \nu \Delta u + cu = F \\ u(\cdot, 0) = u_0 \end{cases} \tag{3.1}$$

The following assumptions are made on the coefficients : $\nu > 0$, $a > 0$, $b \in \mathbb{R}^{n-1}$, $c > 0$. The space variable is $x = (x_1, y)$, $y = (x_2, \cdots, x_n)$. The data u and f are compactly supported in the domain of interest $\Omega_I = (-X, X) \times \mathbb{R}^{n-1}$.

3.1 Transparent boundary condition.

The size of the layer in Figure 2.1 is L. We search for the transparent boundary condition on the exterior side of the layer, $x_1 = X + L$. We perform a Fourier transform in time ($t \leftrightarrow \omega$), and in the tangential variable ($y \leftrightarrow k$) on equation (3.1) for $x_1 \geq X + L$. Since the data u and f are compactly supported in Ω_I, we obtain

$$-\nu\partial_{11}\hat{u} + a\partial_1\hat{u} + (i(\omega + b \cdot k) + \nu|k|^2 + c)\hat{u} = 0, \quad x_1 \geq X + L. \tag{3.2}$$

This can be solved explicitely as

$$\hat{u}(x_1, k, \omega) = \hat{u}(X + L, k, \omega)e^{\lambda^-(x_1 - (X+L))}, \quad x_1 \geq X + L, \tag{3.3}$$

where $\lambda^\pm$ are the roots of the second degree equation

$$-\nu\lambda^2 + a\lambda + (i(\omega + b \cdot k) + \nu|k|^2 + c) = 0, \text{ with } Re\,\lambda^+ > 0, \ Re\,\lambda^- < 0. \tag{3.4}$$

We make an analogous analysis on the left boundary, *i.e.* for $x_1 = -X - L$, and obtain

$$\hat{u}(x_1, k, \omega) = \hat{u}(-X - L, k, \omega) e^{\lambda^+ (x_1 + (X+L))}, \quad x_1 \leq -X - L. \tag{3.5}$$

This analysis provides the transparent boundary conditions

$$\mathcal{B}_{ex}^{\pm} u := \partial_1 u - \Lambda^{\mp}(\partial_y, \partial_t) u = 0, \quad x_1 = \pm(X + L), \tag{3.6}$$

with $\Lambda^{\pm}(ik, i\omega) = \lambda^{\pm}(k, \omega)$, given by

$$\lambda^{\pm}(k, \omega) = \frac{a \pm \delta^{1/2}}{2\nu}, \quad \delta(k, \omega) = a^2 + 4\nu((i(\omega + b \cdot k) + \nu|k|^2 + c), \tag{3.7}$$

which means that solving the advection diffusion equation in $(-X - L, X + L) \times \mathbb{R}^{n-1} \times (0, T)$ with boundary condition (3.6) is equivalent to solving problem (3.1).

3.2 Reflection coefficient.

We consider here a computational boundary on the right only. Suppose we solve the advection diffusion equation in the computational domain with a boundary condition given by

$$\mathcal{B}_a^+ v := \partial_1 v - \Lambda_a^-(\partial_y, \partial_t) v = 0, \qquad x_1 = X + L, \tag{3.8}$$

for Λ_a^- a differential operator whose symbol $\lambda_a^-(k, \omega) = \Lambda_a^-(ik, i\omega)$ is an approximation of Λ^-. Again, by Fourier transform in time and y, we can estimate the error in the domain of interest. Introducing the reflection coefficient

$$R(k, \omega, \lambda_a^-, L) = \frac{\lambda^- - \lambda_a^-}{\lambda^+ - \lambda_a^-} \, e^{(\lambda^- - \lambda^+)L}, \tag{3.9}$$

we have for $x_1 \leq X$,

$$(\hat{u} - \hat{v})(x_1, k, \omega) = R(k, \omega, \lambda_a^-, L) \, \hat{u}(X, k, \omega) \, e^{\lambda^+ (x_1 - X)}. \tag{3.10}$$

Using Paley-Wiener-Schwartz theorem, we have an upper bound for the error in Ω_I, given by

$$\|u - v\|^2_{L^2(\Omega_I \times (0,T))} \leq \int \frac{|R(k, \omega, \lambda_a^-, L)|^2}{2Re\,\lambda^+} |\hat{u}(X, k, \omega)|^2 d\omega \, dk.$$

Since $Re\,\lambda^+ \geq a/\nu$, we obtain

$$\|u - v\|_{L^2(\Omega_I \times (0,T))} \leq \sqrt{\frac{\nu}{2a}} \max_{(\omega,k) \in \mathbb{R}^n} |R(k, \omega, \lambda_a^-, L)| \, \|u(X, \cdot, \cdot)\|_{L^2(\mathbb{R}^{n-1} \times (0,T))}, \tag{3.11}$$

and the same estimate holds for the left boundary. Since $Re\,(\lambda^+ - \lambda^-) \geq a/\nu$, the exponential term in the reflection coefficient ensures its boundedness at infinity. The error in the domain is thus driven by the approximation of λ^- by λ_a^- in the sense defined by the reflection coefficient.

3.3 Old absorbing boundary conditions.

Using a continued fraction expansion, we developed in [5] a series of approximate boundary conditions for $c = 0$, which can be written as $\mathcal{B}_n = \mathcal{B}_1^n$, with $\mathcal{B}_1 = \partial_t + a\partial_1 + b\cdot\nabla_y$. In that case, if v_n is the solution of the advection diffusion equation with $\mathcal{B}_n v_n = 0$ on the exterior boundary of the layer, the error is given by

$$\|u - v_n\|_{L^2(\Omega_I)} \leq \frac{1}{\sqrt{2a}} \nu^{2n+1/2} e^{-\frac{a}{\nu}L} \|\mathcal{L}^{2n} u\|_{L^2(\Omega_I)}.$$

If $\nu \ll 1$, and if we choose $L = Ch$, we get

$$\|u - v_n\|_{L^2(\Omega_I)} \leq \frac{1}{\sqrt{2a}} \nu^{2n+1/2} e^{-2CPe} \|\mathcal{L}^{2n} u\|_{L^2(\Omega_I)},$$

where Pe is the Peclet number, given by $Pe = \frac{ah}{2\nu}$. In the case where ν is not small, we must adopt another strategy, namely the minimization of the reflection coefficient.

3.4 New absorbing boundary conditions

We introduce the complex function

$$f(z) = a^2 + 4\nu c + 4\nu z, \tag{3.12}$$

and $\delta(ik, i\omega) = f(i(\omega + b\cdot k) + \nu|k|^2)$. We now replace $\delta^{1/2}$ in (3.7) by a polynomial $P(i(\omega + b\cdot k) + \nu|k|^2)$, and λ^- by $\lambda_a^- = \frac{a-P}{2\nu}$. This leads to general boundary conditions

$$\mathcal{B}_P^{\pm} u := \partial_1 u - \frac{a}{2\nu} u \pm \frac{1}{2\nu} P(\partial_t + b\cdot\nabla_y - \nu\Delta_y)\, u = 0, x_1 = \pm(X + L) \tag{3.13}$$

For $P(z) = p + qz \in \mathbb{P}_1$, we shall write $\mathcal{B}_{(p,q)}^{\pm}$. It has been proved in [9] that boundary conditions (3.13) lead to well-posed problems when coupled with the advection-diffusion equation in the interior, when the degree of P is zero or 1, and the term Δ_y is not present. Adding that term makes the analysis somewhat more difficult, since we need more regularity, but it does not change the final result. We have not considered higher degree polynomial, or rational fractions.

4 The optimized Schwarz Waveform Relaxation algorithm (SWR).

We introduce two domains $\Omega_1 = (-\infty, L) \times \mathbb{R}^{n-1}$, $\Omega_2 = (0, \infty) \times \mathbb{R}^{n-1}$ as in Figure 2.2, with an overlap of size L. The algorithm computes alternatively the advection diffusion equation in each subdomain on $(0, T)$, and transmits, at the end of the time interval, the information on the interfaces to the neighbour, by

means of two boundary operators $\mathcal{B}^{\pm}(\partial_y, \partial_t)$, as

$$
\left\{
\begin{array}{rcll}
\mathcal{L}(u_1^{n+1}) & = & F & \text{in } \Omega_1 \times (0,T) \\
u_1^{n+1}(\cdot,0) & = & u_0 & \text{in } \Omega_1 \\
\mathcal{B}^+ u_1^{n+1}(L,\cdot) & = & \mathcal{B}^+ u_2^{n}(L,\cdot) & \text{in } (0,T)
\end{array}
\right.
\tag{4.1}
$$
$$
\left\{
\begin{array}{rcll}
\mathcal{L}(u_2^{n+1}) & = & F & \text{in } \Omega_2 \times (0,T) \\
u_2^{n+1}(\cdot,0) & = & u_0 & \text{in } \Omega_2 \\
\mathcal{B}^- u_2^{n+1}(0,\cdot) & = & \mathcal{B}^- u_1^{n}(0,\cdot) & \text{in } (0,T)
\end{array}
\right.
$$

4.1 The optimal Schwarz Waveform Relaxation algorithm.

THEOREM 4.1. *The Schwarz method converges in two iterations with or without overlap when the operators $\mathcal{B}^{\pm}$ are equal to the transparent operators $\mathcal{B}^{\pm}_{ex}$ defined in (3.6).*

This result makes a bridge between Schwarz algorithm and Dirichlet to Neumann operator. Again we approximate the transmission operators.

4.2 Approximate transmission conditions and convergence factor

We approximate λ^- by λ_a^-, as in subsection 3.4, and use in (4.1) the operators $\mathcal{B}_a^{\pm}$ defined in (3.10). Again, it has been proved in [9] that the SWR algorithms with zero or first order transmission conditions with positive coefficients are convergent, both with or without overlap, when the transverse Laplace term is not present.

By Fourier transform in y and t, we can express the errors e_i^k in Ω_i as

$$
\widehat{e_1^{n+2}}(0,k,\omega) = \rho(\omega,k,\lambda_a^-,L)\widehat{e_1^n}(0,k,\omega),
\tag{4.2}
$$

with the convergence factor

$$
\rho(k,\omega,\lambda_a^-,L) = \left(\frac{\lambda^- - \lambda_a^-}{\lambda^+ - \lambda_a^-}\right)^2 e^{(\lambda^- - \lambda^+)L}.
\tag{4.3}
$$

The speed of convergence of the algorithm is driven by the convergence factor. Note that the convergence factor and the reflection coefficient are related by

$$
\rho(k,\omega,\lambda_a^-,L) = R(k,\omega,\lambda_a^-,L/2)^2.
\tag{4.4}
$$

Again, if $\delta^{1/2}$ in (3.7) is replaced by $P(i(\omega + b\cdot k) + \nu|k|^2)$, and $\mathcal{B}^{\pm}$ by $\mathcal{B}_P^{\pm}$, we have a convergence factor

$$
\rho(k,\omega,P,L) = \left(\frac{P - \delta^{1/2}}{P + \delta^{1/2}}\right)^2 e^{-\delta^{1/2}L/\nu};
\tag{4.5}
$$

For P a polynomial of degree lower than 1 with positive coefficients, the rational fraction in ρ has its modulus bounded by 1. Thus we have for L different from zero (the overlapping case) $|\rho(k,\omega,P,L)| \leq e^{-aL/\nu} < 1$, and in the non-overlapping case $|\rho(k,\omega,P,L)| \leq 1$. In any case, Lebesgue's Theorem gives the

convergence result.
As shown in the numerical experiments, it is important to choose P such that ρ or R be as small as possible. We thus are led to the best approximation problem: for a given n, find P in P_n minimizing $\sup_{(\omega,k)\in E} |\rho(\omega, k, P, L)|$. The domain E is a compact set, related to the discretisation, see Section 4.3. This problem has been solved in [2], and explicit formulas for p, q and the convergence rate have been given in the one-dimensional case.

4.3 Asymptotic results in the one-dimensional case

Another strategy could be used for the coefficients p and q in the boundary operators. Large frequencies are damped by the overlap or the absorbing layer, whereas intermediate and small frequencies have to be treated by the transmission condition. So, instead of this difficult approximation problem, it could be tempting to try and use Taylor approximation of $\delta^{1/2}$ in (3.7), for small frequencies ω and k. This would lead to $p = \sqrt{a^2 + 4\nu c}$ for order 0, and $(p, q) = (\sqrt{a^2 + 4\nu c}, 2\nu/\sqrt{a^2 + 4\nu c})$ for order 1 approximation. How do all these reflection or convergence factors behave asymptotically? Suppose a discretization is used with mesh sizes Δt and Δx, which are related by $\Delta t = C_1 \Delta x^\beta$. β is usually 1 or 2, depending on the issue. The boundary layer or overlap is a few cells, *i.e.* $L = C_2 \Delta x$. The set E is $(-\omega_{max}, \omega_{max}) \times (-k_{max}, k_{max})$, with $\omega_{max} = \pi/\Delta t$ and $k_{max} = \pi/\Delta x$. Since ρ tends to 1 for large arguments ω and k, it tends to 1 for small Δx or Δt. Furthermore we have the asymptotic expansions:

Table 4.1: Asymptotic behavior of the convergence rate

method	$\beta = 1$	$\beta = 2$
Taylor order 0	$1 - \mathcal{O}(\Delta x^{1/2})$	$1 - \mathcal{O}(\Delta x^{1/2})$
$\mathbb{P}_0$ optimization	$1 - \mathcal{O}(\Delta x^{1/4})$	$1 - \mathcal{O}(\Delta x^{1/3})$
Taylor order 1	$1 - \mathcal{O}(\Delta x^{1/2})$	$1 - \mathcal{O}(\Delta x^{1/2})$
$\mathbb{P}_1$ optimization	$1 - \mathcal{O}(\Delta x^{1/8})$	$1 - \mathcal{O}(\Delta x^{1/5})$

We can see on this table that for a Taylor approximation, order 0 and order 1 behave asymptotically the same way. $\mathbb{P}_0$ optimization behaves better, and for the $\mathbb{P}_1$ approximation, the convergence rate tends to 1, but very slowly. We can conclude that we discard Taylor approximation, and emphasize $\mathbb{P}_1$ optimization if possible.
Two and three-dimensional asymptotic computations of the coefficients will soon be available.

5 Numerical results

5.1 Absorbing layers

We first present 1-D computations, in order to see the influence of the thickness of the layer. The coefficients in the equation are $a = 1$, $b = 0$, $\nu = 0.2$. The domain of interest is the interval $(0, 3)$, the computation is run on the time interval $(0, 1)$. The initial condition is $u_0 = exp(-10(x - 1.5)^2)$, which is compactly supported in Ω_I. On the left boundary is imposed the value of the free-space solution, so that we compute the error with the values of the exact solution. The numerical scheme is implicit Euler in time with upwinding in space, the mesh sizes are $\Delta t = 1/4000$ and $\Delta x = 1/1000$. We first compare the Neumann boundary condition with the new $\mathbb{P}_0$ optimization. The optimal value is computed with MAPLE, using the equioscillation results in [2]. The error is the relative L^2 norm in time at point $x_1 = X$.

Table 5.1: Relative error on the boundary for two different methods.

size L	0.01	0.02	0.04	0.08	0.16	0.32	0.64
Neumann	0.2832	0.2620	0.2237	0.1615	0.0810	0.0171	0.0011
optimized $\mathcal{B}^+_{(p,0)}$	0.2252	0.1303	0.0570	0.0364	0.0312	0.0094	0.0011

For a very small layer, the relative error is quite large for both methods, whereas as soon as $L \geq 0.04$ (which is about 1 % of the size of the domain), the optimized boundary condition performs much better (by a factor of 5). For very large layers, both methods perform very well, which is not surprising.
We now compare with first order optimized boundary conditions. Again, the optimal value is computed with MAPLE, using the equioscillation results in [2].

Table 5.2: Relative error on the boundary by three different methods.

size L	0.01	0.02	0.04
Neumann	0.2832	0.2620	0.2237
optimized $\mathcal{B}^+_{(p,0)}$	0.2252	0.1303	0.0570
optimized $\mathcal{B}^+_{(p,q)}$	0.0404	0.0342	0.0325

The error is much smaller, even for very small layers. We can even use a layer of size 0.005, that is 5 points. Next table gives the relative error, measured on the boundary or in the L^∞ norm in time and space, in the domain of interest, for the first order optimized boundary condition.

Table 5.3: Relative error for the first order optimized boundary condition.

size L	0.005	0.01	0.02	0.04
L^2 on the boundary	0.0688	0.040	0.0342	0.0325
L^∞ in time and space	0.0279	0.0143	0.0077	0.0070

With ten grid points in the layer, with the first order optimized boundary condition, we reach a 4% precision on the boundary, whereas we need 40 points for the zero order optimized, and 100 for the Neumann boundary condition. With five grid points in the layer, we reach a precision of 3% in the L^∞ norm in time and space.

5.2 Schwarz Waveform Relaxation

One dimensional results have been presented in [2, 6], showing that the continuous properties were preserved by the numerical computations in the case of two subdomains. We show here new results in the case of several subdomains. We use the same model problem as in Section 5.1, and the same numerical scheme. The computational domain is $\Omega = (0, 6)$, the computational time is $T = 2.5$, the initial data is $u(x, 0) = e^{-3(1.5-x)^2}$, and the boundaries are provided with homogeneous Dirichlet data $u(0, t) = 0$ and $u(6, t) = 0$. The mesh sizes are $\Delta x = 0.02$, and $\Delta t = 0.005$. The domain is divided into 8 subdomains, with an overlap of 4 grid points. In Figure 5.1, we show in the top row the first 3 iterations of the classical Schwarz Waveform Relaxation algorithm (which exchanges Dirichlet data on the boundary), and below the same iterations for the algorithm with optimized first order transmission conditions.

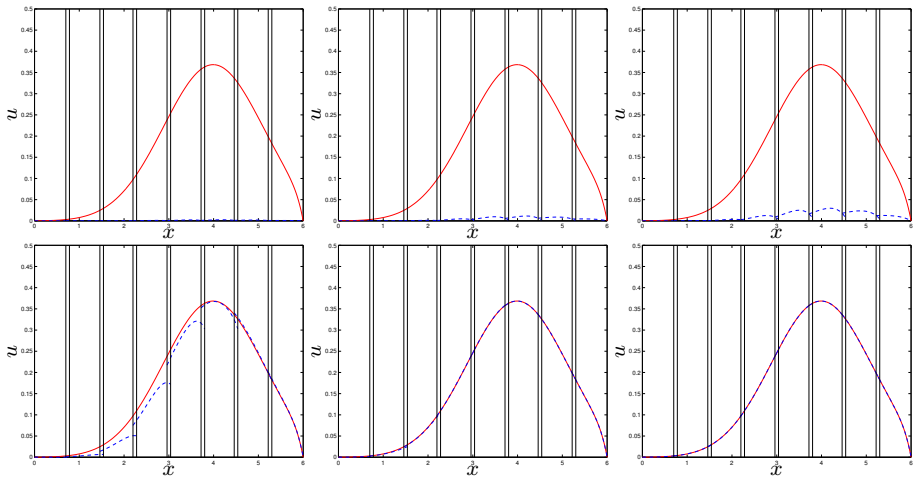

Figure 5.1: From left to right, the first and second iterates $u_j^k(x, T)$, $j = 1, \ldots, 8$ (dashed) at the end of the time interval $t = T$ together with the exact solution (solid).

We show on Figure 5.2 the maximum in time of the error on the interface as a function of the iteration number, for various methods.

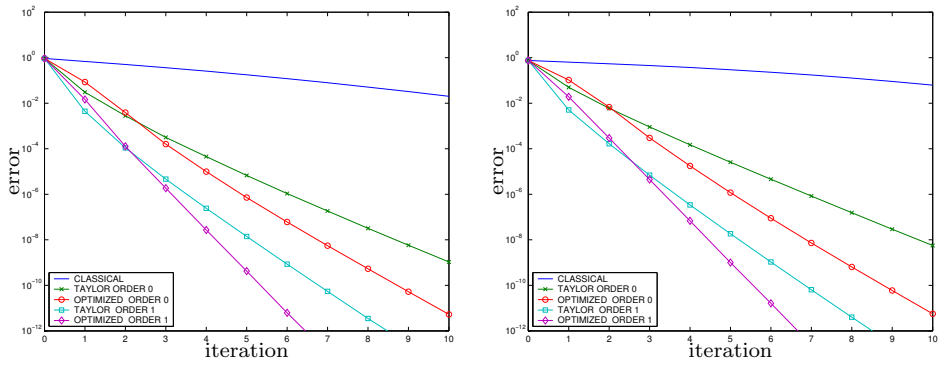

Figure 5.2: Comparison of the methods. **Left:** 4 subdomains, **Right:** 8 subdomains

We clearly see how important the transmission conditions are for the performance of the method. However the number of iterations needed to achieve a certain accuracy does depend of the number of subdomains, as shown on Figure 5.3. It seems to become linear as the number of subdomains increases, see Table 5.4.

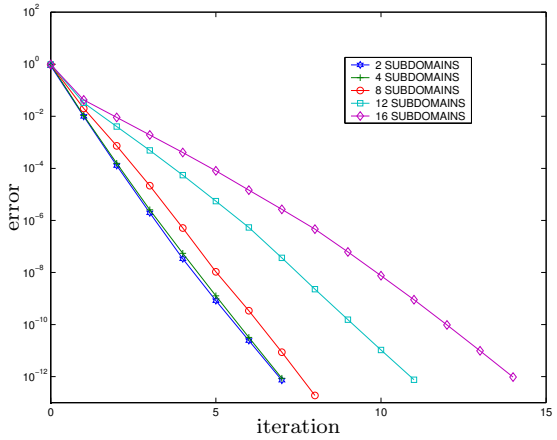

Figure 5.3: Comparison of the performances for the order 1 optimization for various numbers of subdomains.

Table 5.4: Number of iterations needed to achieve an accuracy of 10^{-12} for the first order optimized transmission condition.

Number of subdomains	2	4	8	12	16	20
Number of iterations	7	7	8	11	14	18

5.3 Extension to the coupling of two numerical methods

We show here numerical experiments run in [1]. We compute the evolution of a heat bubble around an airfoil. The domain surrounding the airfoil is computed using finite elements, while the farther field uses finite differences, as shown in Figure 5.4 below. In order to improve the precision, time windows are used. The Schwarz waveform relaxation method was compared to the steady strategy, *i.e.* when the equation is first discretized in time, and a Schwarz algorithm is applied to the resulting elliptic problem. It was noted that the present domain decomposition technique over a time window of 10 time steps converges in terms of number of iterations similarly to 10 preconditioned steady time steps: the Schwarz waveform relaxation acts as a global preconditioner.

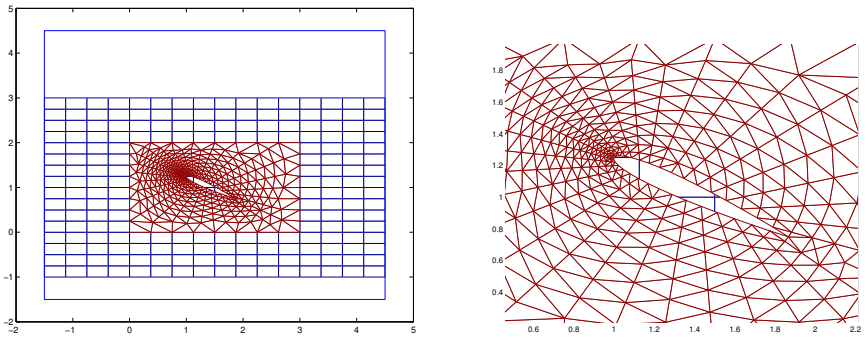

Figure 5.4: Coupling of finite elements and finite differences

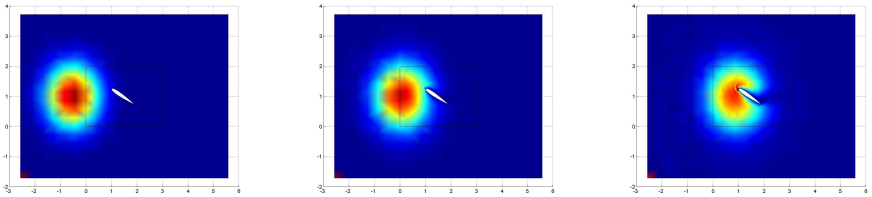

a) T=0 b) T=10 δt c) T=20δt

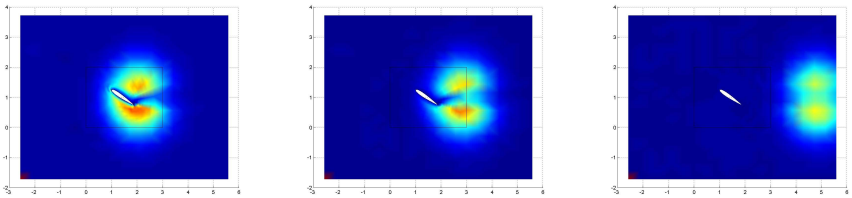

d) T=50δt e) T=70δt f) T=100δt

Figure 5.5: Time evolution of a heat blob around a Naca airfoil. J. Ryan [1].

The full movie can be found at http://www.math.univ-paris13.fr/∼halpern.

5.4 The shallow-water model

This extension was the object of V. Martin's PhD. The full analysis can be found on her web page http://www.mathinfo.u-picardie.fr/martin/.
A first approximation of the viscous linear system is

$$\begin{cases} \dfrac{\partial u}{\partial t} - \nu\triangle u + c^2\dfrac{\partial h}{\partial x} - fv = \dfrac{\tau^x}{\rho_0 H}, \\ \dfrac{\partial v}{\partial t} - \nu\triangle v + c^2\dfrac{\partial h}{\partial y} + fu = \dfrac{\tau^y}{\rho_0 H}, \\ \dfrac{\partial h}{\partial t} + \left(\dfrac{\partial u}{\partial x} + \dfrac{\partial v}{\partial y}\right) = 0, \end{cases}$$

where h is the water height, ν is the viscosity, $f = \beta y$ the Coriolis force, τ the wind force. The transmission conditions on the interfaces are

(5.1)
$$\begin{cases} -\nu\dfrac{\partial u_1^{n+1}}{\partial x} + c^2 h_1^{n+1} - (c + \dfrac{\nu}{c}\dfrac{\partial}{\partial t})u_1^{n+1} = -\nu\dfrac{\partial u_2^n}{\partial x} + c^2 h_2^n - (c + \dfrac{\nu}{c}\dfrac{\partial}{\partial t})u_2^n, \\ -\nu\dfrac{\partial v_1^{n+1}}{\partial x} - pv_1^{n+1} = -\nu\dfrac{\partial v_2^n}{\partial x} - pv_2^n. \end{cases}$$

The free parameter p is obtained by a numerical minmax procedure.
The equations are discretized by a semi implicit finite difference scheme, stabilized by an Asselin filter. It is rewritten through a finite volume procedure,

which enables to take the transmission conditions into account. This amounts to an overlapping algorithm, with one point in the overlap [8]. The domain is $\Omega = (0, L_x) \times (0, L_y)$, $L_x = 15000$ km, $L_y = 3000$ km.. The physical data are $\nu = 500\text{m}^2/\text{s}$, $c = 3$ m/s, $f = \beta y$, $\beta = 2.e^{-11}\text{m}^{-1}\text{s}^{-1}$.The profile of the wind is given by $\tau_y = 0$, $\tau_x = \frac{\tau_0}{2}(1+\tanh(\frac{x_0-x}{d}))$, with $\tau_0 = 5.10^{-2}\text{N/m}^2$, $x_0 = 3000$ km, $d = 300$ km. The mesh sizes are $\Delta t = 30$ mn, $\Delta x = 25$ km, $\Delta y = 15$ km. The time interval $(0, 200d)$ divided into 20 windows, 10 days each.
The Schwarz Waveform Relaxation algorithm is applied to each time window. Figure 5.6 show the convergence history for the classical Schwarz algorithm (with exchange of Dirichlet data on the boundaries), and for the optimized algorithm (5.1). The improvement is really startling.

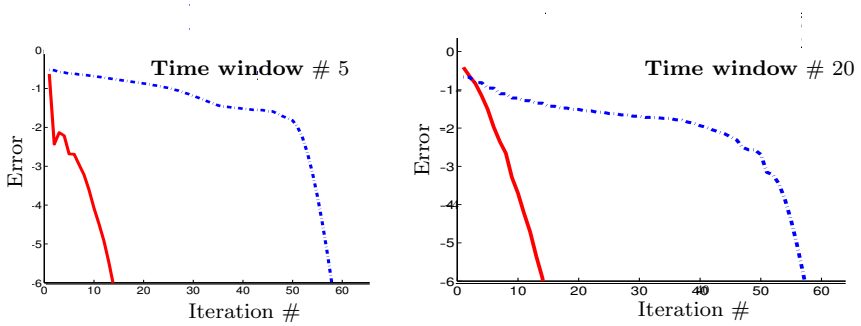

Figure 5.6: Convergence history for the optimized algorithm and the classical algorithm applied to Shallow Water : the L^2 error at the end of the time window as a function of the number of iterations. Dirichlet conditions (dashed) and optimized conditions (solid) V. Martin [8].

6 Conclusion

We have demonstrated the power of the theory of absorbing boundary conditions in the design of absorbing layers and new domain decomposition algorithms. These ideas extend to equations with variable coefficients (many convincing numerical experiments can be found in [9]), and are also used for model coupling [4].

REFERENCES

1. P. D'Anfray , L. Halpern & J. Ryan. *New trends in coupled simulations featuring domain decomposition and metacomputing*. M2AN vol. 36 (5), pp. 953-970, 2002.
2. D. Bennequin, M. J. Gander, and L. Halpern. *Optimized Schwarz Waveform Relaxation methods for convection reaction diffusion problems*. Technical Report 2004-24, LAGA, Université Paris 13, 2004. http://www.math.univ-paris13.fr/prepub/pp2004/pp2004-24.html.

3. B. Engquist and A. Majda. *Absorbing boundary conditions for the numerical simulation of waves.* Math. Comp. vol 31(139), pp 629–651, 1977.
4. M. J. Gander, L. Halpern , C. Japhet and V. Martin, *Advection diffusion problems with pure advection approximation in subregions.* DD16, N.York, january 2004. http://www.ddm.org.
5. L. Halpern, *Artificial boundary conditions for the linear advection diffusion equation.* Math. of Comp vol 46(174), pp. 425-438, 1986.
6. L. Halpern, *Optimized sponge layers, optimized Schwarz Waveform Relaxation algorithms for convection-diffusion problems and best approximation*, DD16, N.York, january 2005. http://www.ddm.org.
7. L. Halpern and J. Rauch, *Absorbing Boundary Conditions for Diffusion Equations.* Numer. Math.,vol 71, pp 185–224,1995.
8. V. Martin *Méthodes de décomposition de domaines de type relaxation d'ondes pour des équations de l'océanographie.* Thèse Université Paris 13. Décembre 2003.
9. V. Martin *An optimized Schwarz Waveform Relaxation method for the unsteady convection diffusion equation in two dimensions.* Appl. Numer. Math. vol 52 (4), pp 401–428, 2005.